World-Grounded Human Motion Recovery via Gravity-View Coordinates

ZEHONG SHEN*, State Key Laboratory of CAD&CG, Zhejiang University, China

HUAIJIN PI*, The University of Hong Kong, China

YAN XIA, State Key Laboratory of CAD&CG, Zhejiang University, China

ZHI CEN, State Key Laboratory of CAD&CG, Zhejiang University, China

SIDA PENG†, Zhejiang University, China

ZECHEN HU, Deep Glint, China

HUJUN BAO, State Key Laboratory of CAD&CG, Zhejiang University, China

RUIZHEN HU, Shenzhen University, China

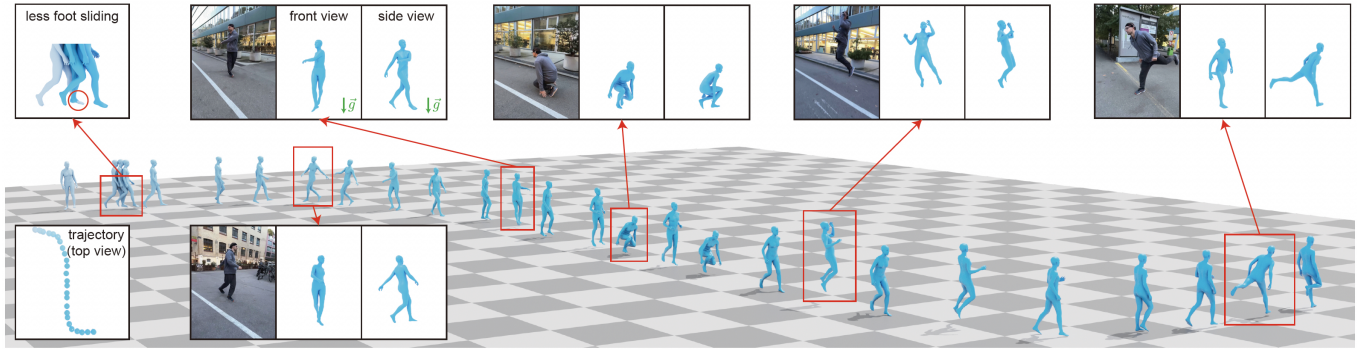XIAOWEI ZHOU, State Key Laboratory of CAD&CG, Zhejiang University, China

Fig. 1. **Overview.** Given an in-the-wild monocular video, our method accurately regresses World-Grounded Human Motion: **4D human poses and shapes in a gravity-aware world coordinate system**. The proposed network, excluding preprocessing (2D human tracking, feature extraction, relative camera rotation estimation), takes 280 ms to process a 1430-frame video (approximately 45 seconds) on an RTX 4090 GPU.

We present a novel method for recovering world-grounded human motion from monocular video. The main challenge lies in the ambiguity of defining the world coordinate system, which varies between sequences. Previous approaches attempt to alleviate this issue by predicting relative motion in an autoregressive manner, but are prone to accumulating errors. Instead, we propose estimating human poses in a novel Gravity-View (GV) coordinate system, which is defined by the world gravity and the camera view direction. The proposed GV system is naturally gravity-aligned and uniquely defined for each video frame, largely reducing the ambiguity of learning image-pose mapping. The estimated poses can be transformed back to the world coordinate system using camera rotations, forming a global motion sequence. Additionally, the per-frame estimation avoids error accumulation in the autoregressive methods. Experiments on in-the-wild benchmarks demonstrate that our method recovers more realistic motion in both the camera space and world-grounded settings, outperforming state-of-the-art methods in both accuracy and speed. The code is available at https://zju3dv.github.io/gvhmr.

CCS Concepts: • **Computing methodologies** → **Motion capture**.

1 INTRODUCTION

World-Grounded Human Motion Recovery (HMR) aims to reconstruct continuous 3D human motion within a gravity-aware world coordinate system. Unlike conventional motion captured in the camera frame [Kanazawa et al. 2018], world-grounded motion is inherently suitable as foundational data for generative and physical models, such as text-to-motion generation [Guo et al. 2022; Tevet et al. 2023] and humanoid robot imitation learning [He et al. 2024]. In these applications, motion sequences must be high-quality and consistent in a gravity-aware world coordinate system.

Most existing HMR methods can recover promising camera-space human motion from videos [Kocabas et al. 2020; Shen et al. 2023; Wei et al. 2022]. To recover the global motion, a straightforward approach is to use camera poses [Teed et al. 2024] to transform camera-space motion to world-space. However, the results are not

*Equal contribution.

†Corresponding author.

guaranteed to be gravity-aligned, and errors in translations and poses can accumulate over time, resulting in implausible global motion. Recent work, WHAM [Shin et al. 2024], attempts to recover global motion by autoregressively predicting relative global poses with RNN. While this method achieves significant improvements, it requires a good initialization and suffers from accumulated errors over long sequences, making it challenging to maintain consistency in the gravity direction. We believe the inherent challenge stems from the ambiguity in defining the world coordinate system. Given the world coordinate axes, any rotation around the gravity axis defines a valid gravity-aware world coordinate system.

In this work, we propose GVHMR to estimate gravity-aware human poses for each frame and then compose them with gravity constraints to avoid accumulated errors in the gravity direction. This design is motivated by the observation that, for a person in any image, we humans are able to easily infer the gravity-aware human pose, as shown in Fig. 2. Additionally, given two consecutive frames, it is intuitively easier to estimate the 1-degree-of-freedom rotation around the gravity direction, compared to the full 3-degree-of-freedom rotation. Therefore, we propose a novel Gravity-View (GV) coordinate system, defined by the gravity and camera view directions. Using the GV system, we develop a network that predicts the gravity-aware human orientation. We also propose a recovery algorithm to estimate the relative rotation between GV systems, enabling us to align all frames into a consistent gravity-aware world coordinate system.

Thanks to the GV coordinates, we can process human rotations in parallel over time. We propose a transformer [Vaswani et al. 2017] model enhanced with Rotary Positional Embedding (RoPE) [Su et al. 2024] to directly regress the entire motion sequence. Compared to the commonly used absolute position encoding, RoPE better captures the relative relationships between video frames and handles long sequences more effectively. During inference, we introduce a mask to limit each frame's receptive field, avoiding the complex sliding windows and enabling parallel inference for infinitely long sequences. Additionally, we predict stationary labels for hands and feet, which are used to refine foot sliding and global trajectories.

In summary, our contributions are threefold: 1. We propose a novel Gravity-View coordinate system and the global orientation recovery method to reduce the cumulative errors in the gravity direction. 2. We develop a Transformer model enhanced by RoPE to generalize to long sequences and improve motion estimation. 3. We demonstrate the effectiveness of our approach through extensive experiments, showing that it outperforms previous methods in both in-camera and world-grounded accuracy.

2 RELATED WORKS

Camera-Space Human Motion Recovery. Recent studies in 3D human recovery predominantly use parametric human models such as SMPL [Loper et al. 2023; Pavlakos et al. 2019]. Given a single image or video, the target is to align the human mesh precisely with the 2D images. Early methods [Bogo et al. 2016; Pavlakos et al. 2019] employ optimization-based approaches by minimizing the repro-jection error. Recently, regression-based methods [Goel et al. 2023; Kanazawa et al. 2018] trained on a large amount of data predict
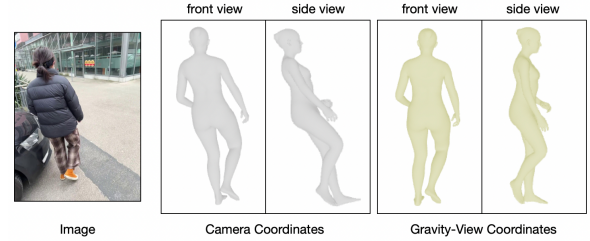

Fig. 2. **Comparison of coordinate systems**. In camera coordinates, a person may appear inclined due to the camera's roll and pitch movement. In contrast, in GV coordinates, the person is naturally aligned with gravity.

the SMPL parameters from the input image directly. Many efforts have been made to improve the accuracy by specialized design architectures [Li et al. 2023; Zhang et al. 2023], part-based reasoning [Kocabas et al. 2021a; Li et al. 2021], and incorporating camera parameters [Kocabas et al. 2021b; Li et al. 2022b]. HMR2.0 [Goel et al. 2023] designs a ViT architecture [Vaswani et al. 2017] and outperforms the previous methods. To utilize temporal cues, [Shi et al. 2020] uses deep networks to predict skeleton pose sequence directly from videos. To recover the human mesh, most methods build upon the HMR pipeline. [Kanazawa et al. 2019] adopts a convolutional encoder. [Choi et al. 2021; Kocabas et al. 2020; Luo et al. 2020] apply RNN successfully. [Sun et al. 2019] introduces self-attention to CNN. [Shen et al. 2023; Wan et al. 2021] employ a transformer encoder to extract temporal information.

Although these methods can accurately estimate human pose, their predictions are all in the camera-space. Consequently, when the camera moves, the human motion becomes physically implausible.

World-Grounded Human Motion Recovery. Traditionally, estimating human motion in a gravity-aware world coordinate system requires additional floor plane calibration or gravity sensors. In multi camera capture systems [Huang et al. 2022; Ionescu et al. 2014], calibration boards are placed on the ground to reconstruct the ground plane and global scale. IMU-based methods [Kaufmann et al. 2023; von Marcard et al. 2018; Yi et al. 2021] use gyroscopes and accelerometers to estimate the gravity direction and then project human motion onto the gravity direction. Recently, researchers put efforts to estimate global human motion from a monocular video. [Yu et al. 2021] reconstructs human motion using physics law but requires a provided scene. Methods like [Li et al. 2022a; Yuan et al. 2022] predicts the global trajectory from locomotion cues. However, the camera motion and human motion are coupled, which make the results noisy. SLAHMR [Ye et al. 2023] and PACE [Kocabas et al. 2024] further integrate SLAM [Teed and Deng 2021; Teed et al. 2024] and pre-learned human motion priors [Rempe et al. 2021] in an optimization framework. Although these methods achieve promising results, the optimization process is time-consuming and faces convergence issues with long video sequences. Furthermore, these methods do not obtain gravity-aligned human motion.

The most relevant work is WHAM [Shin et al. 2024], which directly regresses per-frame pose and translation in an autoregressive manner. However, their method relies on a good initialization and the performance drops in long-term motion recovery due to error
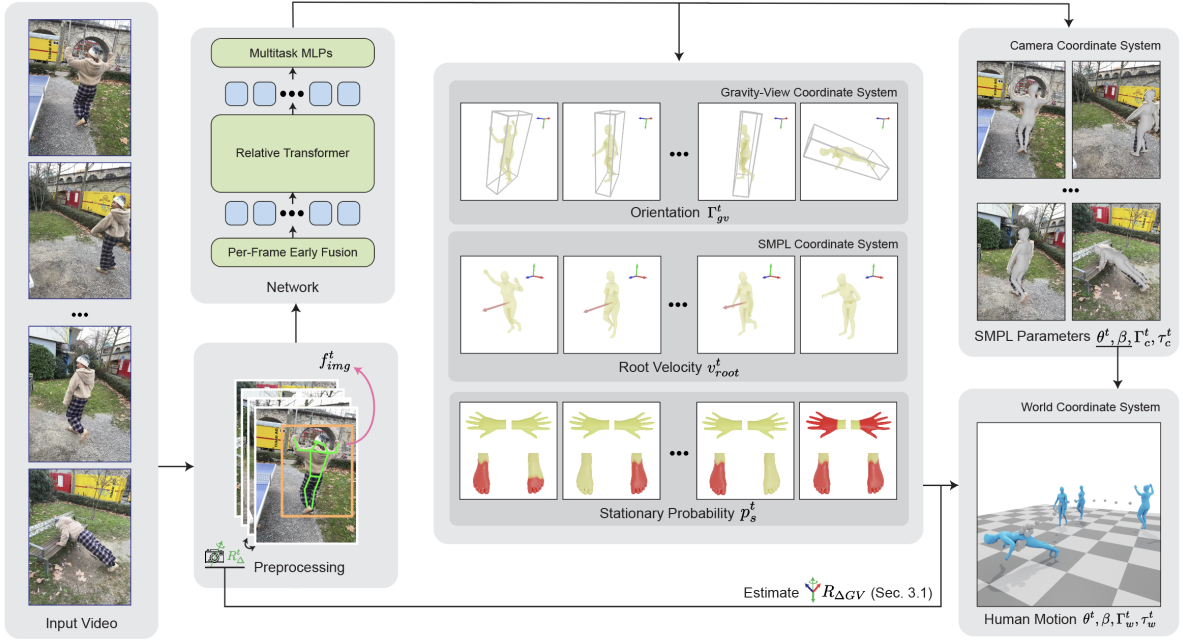
Fig. 3. **Overview of the proposed framework.** Given a monocular video (left), following WHAM [Shin et al. 2024], GVHMR preprocesses the video by tracking the human bounding box, detecting 2D keypoints, extracting image features, and estimating camera relative rotation using visual odometry or a gyroscope. GVHMR then fuses these features into per-frame tokens, which are processed with a relative transformer and multitask MLPs. The outputs include: (1) intermediate representations (middle), i.e. human orientation in the Gravity-View coordinate system, root velocity in the SMPL coordinate system, and the stationary probability for predefined joints; and (2) camera frame SMPL parameters (right-top). Finally, the global trajectory (right-bottom) is recovered by transforming the intermediate representations to the world coordinate system, as described in Sec. 3.1.

accumulation. Two concurrent works also focus on world-grounded human motion recovery. WHAC [Yin et al. 2024] uses visual odometry [Teed et al. 2024] to transform camera coordinate results to a world coordinate system and relies on another network to refine global trajectory. TRAM [Wang et al. 2024] employs SLAM [Teed and Deng 2021] to recover camera motion and uses the scene background to derive the motion scale. They also transform the camera coordinate results into a world coordinate system. In contrast to their methods, GVHMR does not require additional refinement networks and can directly predict the world-grounded human motion.

3 METHOD

Given a monocular video $\{I^t\}_{t=0}^T$, we formulate the task as predicting: (1) the local body poses $\{\theta^t \in \mathbb{R}^{21\times3}\}_{t=0}^T$ and shape coefficients $\beta \in \mathbb{R}^{10}$ of SMPL-X, (2) the human trajectory from SMPL space to the camera space, including the orientation $\{\Gamma_c^t \in \mathbb{R}^3\}_{t=0}^T$ and translation $\{\tau_c^t \in \mathbb{R}^3\}_{t=0}^T$, (3) the trajectory to the world space, including the orientation $\{\Gamma_w^t \in \mathbb{R}^3\}_{t=0}^T$ and translation $\{\tau_w^t \in \mathbb{R}^3\}_{t=0}^T$.

An overview of the proposed pipeline is shown in Fig. 3. In Sec. 3.1, we first introduce the global trajectory representation and discuss its advantages over previous trajectory representations. Then, Sec. 3.2 describes a specially designed network architecture as well as postprocess techniques for predicting the targets. Finally, implementation details are presented in Sec. 3.3.

3.1 Global Trajectory Representation

Global human trajectory $\{\Gamma_w^t, \tau_w^t\}$ refers to the transformation from SMPL space to the *gravity-aware world space* W. However, the definition of W varies, as any rotation of W around the gravity direction is valid, leading to different Γ_w and τ_w. We propose to first recover a gravity-aware human pose for each image, then transform these poses to a consistent global trajectory. This approach is inspired by the observation that humans can easily infer the orientation and gravity direction of a person in an image. And for consecutive frames, estimating the relative rotation around the gravity direction is intuitively easier and more robust.

Specifically, for each image, we use the world gravity direction and the camera's view direction (i.e., the normal vector of the image plane) to define Gravity-View (GV) Coordinates. The proposed new GV coordinate system is mainly used to resolve the rotation ambiguity, so we only predict the per-frame human orientation Γ_{GV}^t relative to the GV system. When the camera moves, we compute the relative rotation between the GV systems of two adjacent frames with relative camera rotations R_Δ^t, thus transforming all Γ_{GV}^t to a consistent gravity-aware global space. For global translation, following [Rempe et al. 2021; Shin et al. 2024], we predict the human displacement in the SMPL coordinate system from time t to $t+1$, and finally roll out in the aforementioned world reference frame.

Gravity-View Coordinate System. As illustrated in Fig. 4, (a) given a person with orientation Γ_c and a gravity direction $\vec{g}$ both described
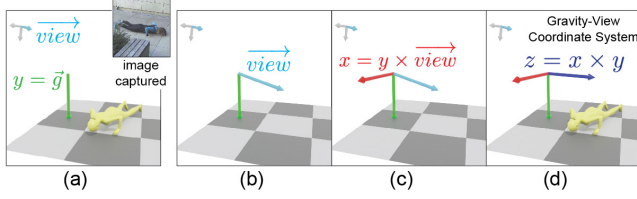
Fig. 4. Gravity-View (GV) coordinate system, defined by the gravity direction and the camera view direction. (Refer to Sec. 3.1 for details).
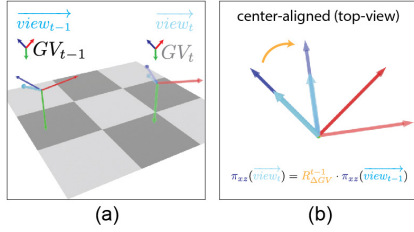

Fig. 5. Relative rotation between two GV coordinate systems. (a) shows two adjacent GV coordinate systems and the camera view directions. (b) illustrates the relative rotation between two GV systems. $R_{\Delta GV}$ occurs **exclusively** around the y-axis (gravity direction).

in the camera space: (b) the y-axis of the GV coordinate system aligns with the gravity direction $\vec{g}$, i.e., $\vec{y} = \vec{g}$; (c) the x-axis is perpendicular to both the camera view direction $\overrightarrow{view} = [0, 0, 1]^T$ and $\vec{y}$ by cross-product, i.e., $\vec{x} = \vec{y} \times \overrightarrow{view}$; (d) finally, the z-axis is calculated by the right-hand rule, i.e., $\vec{z} = \vec{x} \times \vec{y}$. After obtaining these axes, we can re-calculate the person's orientation in the GV coordinate system as our learning target: $\Gamma_{GV} = R_{c2GV} \cdot \Gamma_c = [\vec{x}, \vec{y}, \vec{z}]^T \cdot \Gamma_c$.

Recovering Global Trajectory. It is noteworthy that an independent GV_t exists for each input frame t, where we predict the person's orientation Γ_{GV}^t. To recover a consistent global trajectory $\{\Gamma_w^t, \tau_w^t\}$, all orientations must be transformed to a common reference system. In practice, we use GV_0 as the world reference system W.

To begin with, in the special case of a static camera, the GV_t systems are identical across all frames. Therefore, the human global orientation $\{\Gamma_w^t\}$ is equivalent to $\{\Gamma_{GV}^t\}$. The translation $\{\tau_w^t\}$ is obtained by transforming all predicted local velocities v_{root} into the world coordinate system using the orientations $\{\Gamma_w^t\}$ and then performing a cumulative sum:

$$\tau_w^t = \begin{cases} [0, 0, 0]^T, & t = 0, \\ \sum_{i=0}^{t-1} \Gamma_w^i v_{root}^i, & t > 0. \end{cases} \quad (1)$$

For a moving camera, we first compute the rotation $R_{\Delta GV}^t$ between the GV coordinate systems of frame t to frame $t-1$ by leveraging the input camera relative rotations R_Δ^t, the predicted human orientations Γ_c^t and Γ_{GV}^t. As illustrated in Fig. 5, we first calculate the rotation from camera to GV coordinate system at frame t: $R_{c2gv}^t = \Gamma_{GV}^t \cdot (\Gamma_c^t)^{-1}$. Then, the camera view direction $\overrightarrow{view}_c^t = [0, 0, 1]^T$ is transformed to the GV coordinate system as $\overrightarrow{view}_{GV}^t = R_{c2gv}^t \cdot \overrightarrow{view}_c^t$. We use the camera's relative transformation to rotate this view direction to frame $t-1$, i.e., $\overrightarrow{view}^{t-1} = (R_\Delta^t)^{-1} \cdot \overrightarrow{view}^t$. Since the rotation

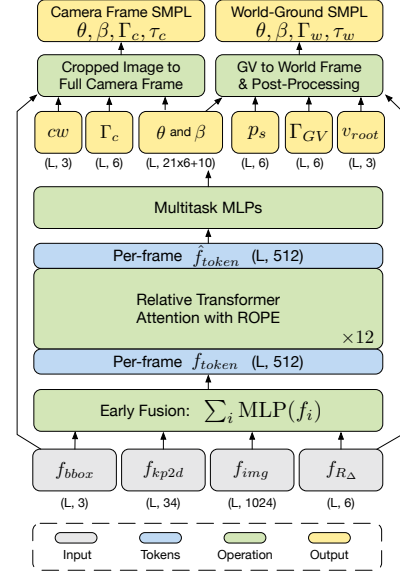**Fig. 6. Network architecture.** The input features are fused into per-frame tokens by the early-fusion module, processed by the relative transformer, and then output by multitask MLPs as intermediate representations. The weak-camera parameter cw is restored to the camera frame τ_c following [Li et al. 2022b]. The predicted Γ_{GV} and v_{root} are converted to the world frame Γ_w and τ_w, as described in Sec. 3.1. Finally, we use joint stationary probabilities p_s to post-process the global motion.

between the GV_t systems is always around the gravity vector, we can calculate the rotation matrix $R_{\Delta GV}^t$ by projecting the view directions $\overrightarrow{view}^{t-1}$ and $\overrightarrow{view}^t$ onto the xz-plane and computing the angle between them. After obtaining $\{R_{\Delta GV}^t\}$ of the entire input sequences, we can roll out to the first frame's GV coordinate system for all frames:

$$\Gamma_w^t = \begin{cases} \Gamma_{GV}^0, & t = 0, \\ \Pi_{i=1}^t R_{\Delta GV}^i \cdot \Gamma_{GV}^t, & t > 0. \end{cases} \quad (2)$$

This formulation also applies to static cameras, as the transformation $R_{\Delta GV}^t$ is the identity transformation in this case. Finally, the translation is obtained using the same method as described in Eq. 1.

The human orientation in the GV coordinate system is well-suited for deep network learning, given that the establishment of the GV coordinate system is determined from the input images. It also ensures that the learned global orientation is naturally gravity-aware. We have also found this approach beneficial for learning local pose and shape, as demonstrated in the ablation study Tab. 3. In the rotation recovery algorithm between GV systems, we utilize the consistency of the y-axis in the GV system to systematically avoid cumulative errors in the gravity direction. This also mitigates potential errors in camera rotation estimation, resulting in our method achieving similar results under both GT Gyro and DPVO estimated relative camera rotations, as shown in Tab. 1. Compared to WHAM, our method does not require initialization and can predict in parallel without the need for autoregressive prediction.

3.2 Network Design

Input and preprocessing. The network design is shown in Fig. 6. Inspired by WHAM [Shin et al. 2024], we first preprocess the input video into four types of features: bounding boxes[Jocher et al. 2023; Li et al. 2022b], 2D keypoints [Xu et al. 2022], image features [Goel et al. 2023], and relative camera rotations [Teed et al. 2024]. Then, in the early-fusion module, we use individual MLPs to map these features to the same dimension. These vectors are then element-wise added to obtain per-frame tokens $\{f_{\text{token}}^t \in \mathbb{R}^{512}\}$. These tokens are processed by a Relative Transformer, where we introduce rotary positional encoding (RoPE) [Su et al. 2024] to enable the network to focus on relative position features. Additionally, we implement a receptive-field-limited attention mask to improve the network's generalization ability when testing on long sequences.

Rotary positional embedding. Absolute positional embedding is a common approach for transformer architectures in human motion modeling. However, this implicitly reduces the model's ability to generalize to long sequences because the model is not trained on positional encodings beyond the training length. We argue that the absolute position of human motions is ambiguous (e.g., the start of a motion sequence can be arbitrary). In contrast, the relative position is well-defined and can be easily learned.

Here we introduce rotary positional embedding to inject relative features into temporal tokens, where the output $\mathbf{o}^t$ of the t-th token after the self-attention layer is calculated via:

$$\mathbf{o}^t = \sum_{i \in T} \underset{s \in T}{\text{Softmax}} \left(a^{ts}\right)^i \mathbf{W}_v f_{token}^i \quad (3)$$

$$a^{ts} = (\mathbf{W}_q f_{token}^t)^\top \mathbf{R}\left(\mathbf{p}^s - \mathbf{p}^t\right)(\mathbf{W}_k f_{token}^s) \quad (4)$$

where $\mathbf{W_q}$, $\mathbf{W_k}$, $\mathbf{W_v}$ are the projection matrix, $\mathbf{R}(\cdot) \in \mathbb{R}^{512 \times 512}$ is the rotary encoding of the relative position between two tokens, and $\mathbf{p}^t$ indicates the temporal index of the t-th token. Following the definition in RoPE, we divide the 512-dimensional space into 256 subspaces and combine them using the linearity of the inner product. $\mathbf{R}(\cdot)$ is defined as:

$$\mathbf{R}(\mathbf{p}) = \begin{pmatrix} \hat{\mathbf{R}}\left(\alpha_1^\top \mathbf{p}\right) & & \mathbf{0} \\ & \ddots & \\ \mathbf{0} & & \hat{\mathbf{R}}\left(\alpha_{256}^\top \mathbf{p}\right) \end{pmatrix}, \hat{\mathbf{R}}(\theta) = \begin{pmatrix} \cos\theta & -\sin\theta \\ \sin\theta & \cos\theta \end{pmatrix},$$
$$(5)$$

where α_i is pre-defined frequency parameters.

At inference time, we further introduce an attention mask [Press et al. 2022] and the self-attention becomes:

$$\mathbf{o}^t = \sum_{i \in T} \underset{s \in T}{\text{Softmax}} \left(a^{ts} + m^{ts}\right)^i \mathbf{W}_v f_{token}^i \quad (6)$$

$$m^{ts} = \begin{cases} 0, & \text{if } -L < t - s < L, \\ -\infty, & \text{otherwise.} \end{cases} \quad (7)$$

where L is the maximum training length. The token t attends only to tokens within L relative positions. Consequently, the model can generalize to arbitrarily long sequences without needing autoregressive inference techniques, such as sliding-window.

Network outputs. After the relative transformer, the f'_{token} are processed by multitask MLPs to predict multiple targets, including the weak-perspective camera parameters cw, the human orientation in the camera frame Γ_c, the SMPL local pose θ, the SMPL shape β, the stationary label p_j, the global trajectory representation Γ_{GV} and v_{root}. To get the camera-frame human motion, we follow the standard CLIFF [Li et al. 2022b] to transform the weak-perspective camera to full-perspective. For the world-grounded human motion, we recover the global trajectory as described in Sec. 3.1.

Post-processing. The proposed network learns smooth and realistic global movement from the training data. Inspired by WHAM, we additionally predict joint stationary probabilities to further refine the global motion. Specifically, we predict the stationary probabilities for the hands, toes, and heels, and then update the global translation frame-by-frame to ensure that the static joints remain at fixed points in space as much as possible. After updating the global translation, we calculate the fine-grained stationary positions for each joint (see the algorithm in the supplementary). These target joint positions are then passed into an inverse kinematics process to solve the local poses, mitigating physically implausible effects like foot-sliding. We use a CCD-based IK solver [Aristidou and Lasenby 2011] with an efficient implementation [Starke et al. 2019].

Losses. We use the following losses for training: Mean Squared Error (MSE) loss on predicted targets except for stationary probability, which uses Binary Cross-Entropy (BCE) loss. Additionally, we use L2 loss on 3D joints, 2D joints, vertices, translation in the camera frame, and translation in the world coordinate system. More details are provided in the supplementary material.

3.3 Implementation details

GVHMR has 12 layers of transformer encoder. Each attention unit has 8 heads. The hidden dimension is 512. The MLP has two linear layers with GELU activation. GVHMR is trained from scratch on a mixed dataset consisting of AMASS [Mahmood et al. 2019], BED-LAM [Black et al. 2023], H36M [Ionescu et al. 2014], and 3DPW [von Marcard et al. 2018]. During training, we augment the 2D keypoints following WHAM. For AMASS, we simulate static and dynamic camera trajectories, generate bounding boxes, normalize the key-points using these boxes from -1 to 1, and set image features to zero. For other datasets that come with videos, we extract image features using a fixed encoder [Goel et al. 2023]. The training sequence length is set to $L = 120$. The model converges after 500 epochs with a batch size of 256. Training takes 13 hours on 2 RTX 4090 GPUs.

4 EXPERIMENTS

4.1 Datasets and Metrics

Evaluation datasets. Following WHAM [Shin et al. 2024], we evaluate our method on three in-the-wild benchmarks: 3DPW [von Marcard et al. 2018], RICH [Huang et al. 2022], EMDB [Kaufmann et al. 2023]. We use RICH and EMDB-2 split to evaluate the global performance. The RICH test set contains 191 videos captured with static cameras, totaling 59.1 minutes with accurate global human motion annotations. The EMDB-2 is captured with moving cameras and contains 25 sequences totaling 24.0 minutes. Additionally,

Table 1. **World-grounded metrics.** We evaluate the global motion quality on the RICH [Huang et al. 2022] and EMDB-2 [Kaufmann et al. 2023] dataset. Parenthesis denotes the number of joints used to compute WA-MPJPE$_{100}$, W-MPJPE$_{100}$ and Jitter.

Models	RICH (24)					EMDB (24)				
	WA-MPJPE$_{100}$	W-MPJPE$_{100}$	RTE	Jitter	Foot-Sliding	WA-MPJPE$_{100}$	W-MPJPE$_{100}$	RTE	Jitter	Foot-Sliding
DPVO[Teed et al. 2024] +HMR2.0[Goel et al. 2023]	184.3	338.3	7.7	255.0	38.7	647.8	2231.4	15.8	537.3	107.6
GLAMR [Yuan et al. 2022]	129.4	236.2	3.8	49.7	18.1	280.8	726.6	11.4	46.3	20.7
TRACE [Sun et al. 2023]	238.1	925.4	610.4	1578.6	230.7	529.0	1702.3	17.7	2987.6	370.7
SLAHMR [Ye et al. 2023]	98.1	186.4	28.9	34.3	5.1	326.9	776.1	10.2	31.3	14.5
WHAM (w/ DPVO) [Shin et al. 2024]	109.9	184.6	4.1	19.7	3.3	135.6	354.8	6.0	22.5	4.4
WHAM (w/ GT gyro) [Shin et al. 2024]	109.9	184.6	4.1	19.7	3.3	131.1	335.3	4.1	21.0	4.4
Ours (w/ DPVO)	**78.8**	**126.3**	**2.4**	**12.8**	**3.0**	111.0	276.5	2.0	16.7	**3.5**
Ours (w/ GT gyro)	**78.8**	**126.3**	**2.4**	**12.8**	**3.0**	**109.1**	**274.9**	**1.9**	**16.5**	**3.5**

Table 2. **Camera-space metrics.** We evaluate the camera-space motion quality on the 3DPW [von Marcard et al. 2018], RICH [Huang et al. 2022] and EMDB-1 [Kaufmann et al. 2023] datasets. * denotes models trained with the 3DPW training set.

	Models	3DPW (14)				RICH (24)				EMDB (24)			
		PA-MPJPE	MPJPE	PVE	Accel	PA-MPJPE	MPJPE	PVE	Accel	PA-MPJPE	MPJPE	PVE	Accel
per-frame	SPIN [Kolotouros et al. 2019]	59.2	96.9	112.8	31.4	69.7	122.9	144.2	35.2	87.1	140.3	174.9	41.3
	PARE* [Kocabas et al. 2021a]	46.5	74.5	88.6	–	60.7	109.2	123.5	–	72.2	113.9	133.2	–
	CLIFF* [Li et al. 2022b]	43.0	69.0	81.2	22.5	56.6	102.6	115.0	22.4	68.1	103.3	128.0	24.5
	HybrIK* [Li et al. 2021]	41.8	71.6	82.3	–	56.4	96.8	110.4	–	65.6	103.0	122.2	–
	HMR2.0 [Goel et al. 2023]	44.4	69.8	82.2	18.1	48.1	96.0	110.9	18.8	60.6	98.0	120.3	19.8
	ReFit* [Wang and Daniilidis 2023]	40.5	65.3	75.1	18.5	47.9	80.7	92.9	17.1	58.6	88.0	104.5	20.7
temporal	TCMR* [Choi et al. 2021]	52.7	86.5	101.4	6.0	65.6	119.1	137.7	5.0	79.6	127.6	147.9	5.3
	VIBE* [Kocabas et al. 2020]	51.9	82.9	98.4	18.5	68.4	120.5	140.2	21.8	81.4	125.9	146.8	26.6
	MPS-Net* [Wei et al. 2022]	52.1	84.3	99.0	6.5	67.1	118.2	136.7	5.8	81.3	123.1	138.4	6.2
	GLoT* [Shen et al. 2023]	50.6	80.7	96.4	6.0	65.6	114.3	132.7	5.2	78.8	119.7	138.4	5.4
	GLAMR [Yuan et al. 2022]	51.1	–	–	8.0	79.9	–	–	107.7	73.5	113.6	133.4	32.9
	TRACE* [Sun et al. 2023]	50.9	79.1	95.4	28.6	–	–	–	–	70.9	109.9	127.4	25.5
	SLAHMR [Ye et al. 2023]	55.9	–	–	–	52.5	–	–	9.4	69.5	93.5	110.7	7.1
	PACE [Kocabas et al. 2024]	–	–	–	–	49.3	–	–	8.8	–	–	–	–
	WHAM* [Shin et al. 2024]	**35.9**	57.8	68.7	6.6	44.3	80.0	91.2	5.3	50.4	79.7	94.4	5.3
	Ours*	36.2	**55.6**	**67.2**	**5.0**	**39.5**	**66.0**	**74.4**	**4.1**	**42.7**	**72.6**	**84.2**	**3.6**

we use RICH, EMDB-1 split, and 3DPW to evaluate the camera-coordinate performance. EMDB-1 contains 17 sequences totaling 13.5 minutes, and 3DPW contains 37 sequences totaling 22.3 minutes. We also test our method on internet videos for qualitative results (see supplementary video).

Metrics. We follow the evaluation protocol of [Shin et al. 2024; Ye et al. 2023], using the code released by WHAM to apply FlipEval for test-time augmentation and evaluate our model's performance. To compute world-coordinate metrics, we divide the predicted global sequences into shorter segments of 100 frames and align each segment to the ground-truth segment. When the alignment is performed using the entire segment, we report the World-aligned Mean Per Joint Position Error (WA-MPJPE$_{100}$). When the alignment is performed using the first two frames, we report the World MPJPE (W-MPJPE$_{100}$). Additionally, to assess the error over the global motion, we evaluate the whole sequence for Root Translation Error (RTE, in %), motion jittery (Jitter, in m/s^3), and foot sliding (FS, in mm). The camera-coordinate metrics include the widely used MPJPE, Procrustes-aligned MPJPE (PA-MPJPE), Per Vertex Error (PVE), and Acceleration error (Accel, in m/s^2) [Goel et al. 2023; Li et al. 2022b; Shin et al. 2024; Ye et al. 2023].

4.2 Comparison on Global Motion Recovery

We compare our method with several state-of-the-art methods that recover global motion and a straightforward baseline method that combines the state-of-the-art camera-space method HMR2.0 [Goel et al. 2023] with a SLAM method (DPVO [Teed et al. 2024]). The GT gyro indicates the ground-truth camera rotation data in the EMDB dataset provided by the ARKit. For the static camera in the RICH dataset, we set the camera transformation to an identity matrix.

As illustrated in Tab. 1, our method achieves the best performance on all metrics. Compared to WHAM, we can better handle errors in relative camera rotation estimation. On the EMDB dataset with dynamic camera inputs, using DPVO instead of Gyro results in only a 1.6mm/0.1% drop in the W-MPJPE$_{100}$/RTE metrics, while WHAM experiences a drop of 19.5mm/1.9%. Compared to optimization-based algorithms like GLAMR and SLAHMR, our method also achieves better smoothness metrics. Although these methods incorporate a smoothness loss, they may struggle due to the high difficulty of the actions in the dataset. Compared to regression methods like TRACE, our algorithm generalizes better to new datasets and achieves superior results. An important baseline is HMR2.0+DPVO. We found that, although HMR2.0 performs well in camera-space Tab. 2, it performs

Table 3. **Ablation studies**. We compare our method with seven variants on the RICH [Huang et al. 2022] dataset (Refer to Sec. 4.4 for details). * denotes the variant that employs the sliding window.

Variant	PA-MPJPE	MPJPE	WA-MPJPE	W-MPJPE	RTE	Jitter	Foot-Sliding
(1) w/o GV	40.0	67.0	162.6	278.9	5.9	9.7	7.5
(2) w/o Γ_{GV}	41.4	70.5	101.2	177.5	4.5	14.9	3.0
(3) w/o Transformer	43.3	73.9	85.8	138.9	2.7	**7.6**	3.3
(4) w/o Transformer*	43.0	72.9	84.2	142.0	2.7	10.6	3.2
(5) w/o RoPE	87.5	172.9	191.5	304.4	6.3	22.8	11.5
(6) w/o RoPE*	40.1	67.9	80.7	133.2	2.4	17.5	3.3
(7) w/o PostProcessing	39.5	66.0	89.3	145.2	3.0	14.5	6.8
Full Model	**39.5**	**66.0**	**78.8**	**126.3**	**2.4**	12.8	**3.0**

Table 4. **Dataset and test-time-augmentation ablation on EMDB**. B denotes BEDLAM [Black et al. 2023] synthetic dataset.

Method	PA-MPJPE	MPJPE	Accel	WA-MPJPE	W-MPJPE	RTE
WHAM +B	49.4	78.2	6.0	134.2	338.1	3.8
WHAM +B+FlipEval	47.9	76.9	5.4	132.5	337.7	3.8
GVHMR +B	44.2	74.0	4.0	110.6	274.9	1.9
GVHMR +B+FlipEval	42.7	72.6	3.6	109.1	272.9	1.9

poorly in global motion recovery. Particularly on the RICH dataset, the camera transformation is identity, indicating that camera-space estimation of human pose struggles to recover correct and consistent translation and scale. Additionally, such methods cannot achieve gravity-aligned results. In contrast, our algorithm naturally provides gravity-aligned results.

As shown in Fig. 7, our method can recover more plausible global motion than WHAM. To validate the effectiveness of our method, we show the global orientation angle error curve in Fig. 9. It can be observed that our method maintains a much lower error than WHAM, especially in the long-term prediction.

4.3 Comparison on Camera Space Motion Recovery

We compare our method with state-of-the-art motion recovery methods that predict camera-space results. The results are shown in Tab. 2, where our method achieves the best performance on most of the metrics with a clear margin, demonstrating the effectiveness of our method in camera-space motion recovery. We attribute this to the multitask learning strategy that enables our model to use global motion information to improve the camera-space motion estimation, especially the shape and smoothness of the motion. Our PA-MPJPE performance is slightly behind WHAM by 0.3 mm on the 3DPW dataset. This may be due to the fact that we do not directly predict the SMPL parameters, but rather the SMPLX parameters, which might introduce some errors. Nevertheless, the numbers are still competitive. Fig. 8 demonstrates that our approach estimates human motion in the camera space more accurately than WHAM.

4.4 Understanding GVHMR

Ablation Studies. To understand the impact of each component in our method, we evaluate seven variants of GVHMR using the same training and evaluation protocol on the RICH dataset. The results are shown in Tab. 3: (1) *w/o GV*: when predicting human motion solely in the camera coordinate system, the metrics drop slightly. This suggests that gravity alignment improves camera-space human motion estimation accuracy. For this variant, we can further recover a non-gravity-aligned global motion, which performs poorly in global metrics. (2) *w/o Γ_{GV}*: when predicting the relative global orientation from frame to frame, the world-coordinate metrics drop substantially, indicating that the model suffers from error accumulation in this configuration. (3) *w/o Transformer*: adopting a convolutional architecture yields poor performance, highlighting that our transformer architecture is more effective. (4) *w/o Transformer**: when applying a convolutional architecture with a sliding window

inference strategy, the performance remains similarly poor, further validating the superiority of our transformer approach. (5) *w/o RoPE*: substituting RoPE with absolute positional encoding leads to very poor results. This is primarily because absolute positional embedding struggles to generalize well in long sequences. (6) *w/o RoPE**: even when using absolute positional embedding with a sliding window inference strategy, the results are still worse than our approach, confirming the inadequacy of this embedding strategy. (7) *w/o Post-Processing*: Omitting the postprocessing step causes a significant increase in global metrics, demonstrating that our postprocessing strategy substantially enhances global accuracy. Fig. 10 demonstrates that each component of our approach contributes to the overall performance. We find similar conclusion on the EMDB dataset, which is presented in the supplementary material.

In Tab. 4, we provide a comparison with the most relevant baseline method, WHAM. When trained on the BEDLAM dataset, with or without using FlipEval as a test-time augmentation, GVHMR shows a significant performance improvement over WHAM. Additionally, we observe that FlipEval offers greater improvements in camera-space metrics compared to global-space metrics.

Running Time. We test the running time with an example video of 1430 frames (approximately 45 seconds). The preprocessing, which includes YOLOv8 detection, ViTPose, Vit feature extraction, and DPVO, takes a total of 46.0 seconds (4.9 + 20.0 + 10.1 + 11.0). The rest of the GVHMR takes 0.28 seconds. WHAM adopts the same preprocessing procedures, and it requires 2.0 seconds for the core network. The optimization-based method SLAHMR takes more than 6 hours to process. All models are tested with an RTX 4090 GPU. The improved efficiency enables scalable processing of human motion videos, aiding in the creation of foundational datasets.

5 CONCLUSIONS

We introduce GVHMR , a novel approach for regressing world-grounded human motion from monocular videos. GVHMR defines a Gravity-View (GV) coordinate system to leverage gravity priors and constraints, avoiding error accumulation along the gravity axis. By incorporating a relative transformer with RoPE, GVHMR handles sequences of arbitrary length during inference, without the need for sliding-window. Extensive experiments demonstrate that GVHMR outperforms existing methods across various benchmarks, achieving state-of-the-art accuracy and motion plausibility in both camera-space and world-grounded metrics.

REFERENCES

Andreas Aristidou and Joan Lasenby. 2011. FABRIK: A fast, iterative solver for the Inverse Kinematics problem. *Graphical Models* 73, 5 (2011), 243–260.

Michael J. Black, Priyanka Patel, Joachim Tesch, and Jinlong Yang. 2023. BEDLAM: A Synthetic Dataset of Bodies Exhibiting Detailed Lifelike Animated Motion. In *Proceedings IEEE/CVF Conf. on Computer Vision and Pattern Recognition (CVPR)*. 8726–8737.

Federica Bogo, Angjoo Kanazawa, Christoph Lassner, Peter Gehler, Javier Romero, and Michael J. Black. 2016. Keep it SMPL: Automatic Estimation of 3D Human Pose and Shape from a Single Image. In *Computer Vision – ECCV 2016 (Lecture Notes in Computer Science)*. Springer International Publishing, 561–578.

Hongsuk Choi, Gyeongsik Moon, Ju Yong Chang, and Kyoung Mu Lee. 2021. Beyond Static Features for Temporally Consistent 3D Human Pose and Shape from a Video. In *Conference on Computer Vision and Pattern Recognition (CVPR)*.

Shubham Goel, Georgios Pavlakos, Jathushan Rajasegaran, Angjoo Kanazawa, and Jitendra Malik. 2023. Humans in 4D: Reconstructing and tracking humans with transformers. In *Proceedings of the IEEE/CVF International Conference on Computer Vision*. 14783–14794.

Chuan Guo, Shihao Zou, Xinxin Zuo, Sen Wang, Wei Ji, Xingyu Li, and Li Cheng. 2022. Generating diverse and natural 3d human motions from text. In *Proceedings of the IEEE/CVF Conference on Computer Vision and Pattern Recognition*. 5152–5161.

Tairan He, Zhengyi Luo, Wenli Xiao, Chong Zhang, Kris Kitani, Changliu Liu, and Guanya Shi. 2024. Learning Human-to-Humanoid Real-Time Whole-Body Teleoperation. In *arXiv*.

Chun-Hao P. Huang, Hongwei Yi, Markus Höschle, Matvey Safroshkin, Tsvetelina Alexiadis, Senya Polikovsky, Daniel Scharstein, and Michael J. Black. 2022. Capturing and Inferring Dense Full-Body Human-Scene Contact. In *Proceedings IEEE/CVF Conf. on Computer Vision and Pattern Recognition (CVPR)*. 13274–13285.

Catalin Ionescu, Dragos Papava, Vlad Olaru, and Cristian Sminchisescu. 2014. Human3.6M: Large Scale Datasets and Predictive Methods for 3D Human Sensing in Natural Environments. *IEEE Transactions on Pattern Analysis and Machine Intelligence* 36, 7 (jul 2014), 1325–1339.

Glenn Jocher, Ayush Chaurasia, and Jing Qiu. 2023. *Ultralytics YOLOv8*. https://github.com/ultralytics/ultralytics

Angjoo Kanazawa, Michael J. Black, David W. Jacobs, and Jitendra Malik. 2018. End-to-end Recovery of Human Shape and Pose. In *Computer Vision and Pattern Regognition (CVPR)*.

Angjoo Kanazawa, Jason Y Zhang, Panna Felsen, and Jitendra Malik. 2019. Learning 3d human dynamics from video. In *Proceedings of the IEEE/CVF conference on computer vision and pattern recognition*. 5614–5623.

Manuel Kaufmann, Jie Song, Chen Guo, Kaiyue Shen, Tianjian Jiang, Chengcheng Tang, Juan José Zárate, and Otmar Hilliges. 2023. EMDB: The Electromagnetic Database of Global 3D Human Pose and Shape in the Wild. In *International Conference on Computer Vision (ICCV)*.

Muhammed Kocabas, Nikos Athanasiou, and Michael J. Black. 2020. VIBE: Video Inference for Human Body Pose and Shape Estimation. In *Proceedings IEEE Conf. on Computer Vision and Pattern Recognition (CVPR)*. IEEE, 5252–5262. https://doi.org/10.1109/CVPR42600.2020.00530

Muhammed Kocabas, Chun-Hao P. Huang, Otmar Hilliges, and Michael J. Black. 2021a. PARE: Part Attention Regressor for 3D Human Body Estimation. In *Proc. International Conference on Computer Vision (ICCV)*. 11127–11137.

Muhammed Kocabas, Chun-Hao P. Huang, Joachim Tesch, Lea Müller, Otmar Hilliges, and Michael J. Black. 2021b. SPEC: Seeing People in the Wild with an Estimated Camera. In *Proc. International Conference on Computer Vision (ICCV)*. IEEE, Piscataway, NJ, 11015–11025. https://doi.org/10.1109/ICCV48922.2021.01085

Muhammed Kocabas, Ye Yuan, Pavlo Molchanov, Yunrong Guo, Michael J. Black, Otmar Hilliges, Jan Kautz, and Umar Iqbal. 2024. PACE: Human and Motion Estimation from in-the-wild Videos. In *3DV*.

Nikos Kolotouros, Georgios Pavlakos, Michael J Black, and Kostas Daniilidis. 2019. Learning to Reconstruct 3D Human Pose and Shape via Model-fitting in the Loop. In *ICCV*.

Jiefeng Li, Siyuan Bian, Qi Liu, Jiasheng Tang, Fan Wang, and Cewu Lu. 2023. NIKI: Neural Inverse Kinematics with Invertible Neural Networks for 3D Human Pose and Shape Estimation. In *Proceedings of the IEEE/CVF Conference on Computer Vision and Pattern Recognition (CVPR)*.

Jiefeng Li, Siyuan Bian, Chao Xu, Gang Liu, Gang Yu, and Cewu Lu. 2022a. D &d: Learning human dynamics from dynamic camera. In *European Conference on Computer Vision*. Springer, 479–496.

Jiefeng Li, Chao Xu, Zhicun Chen, Siyuan Bian, Lixin Yang, and Cewu Lu. 2021. Hybrik: A hybrid analytical-neural inverse kinematics solution for 3d human pose and shape estimation. In *Proceedings of the IEEE/CVF Conference on Computer Vision and Pattern Recognition*. 3383–3393.

Zhihao Li, Jianzhuang Liu, Zhensong Zhang, Songcen Xu, and Youliang Yan. 2022b. CLIFF: Carrying Location Information in Full Frames into Human Pose and Shape Estimation. In *ECCV*.

Matthew Loper, Naureen Mahmood, Javier Romero, Gerard Pons-Moll, and Michael J Black. 2023. SMPL: A skinned multi-person linear model. In *Seminal Graphics Papers: Pushing the Boundaries, Volume 2*. 851–866.

Zhengyi Luo, S. Alireza Golestaneh, and Kris M. Kitani. 2020. 3D Human Motion Estimation via Motion Compression and Refinement. In *Proceedings of the Asian Conference on Computer Vision (ACCV)*.

Naureen Mahmood, Nima Ghorbani, Nikolaus F. Troje, Gerard Pons-Moll, and Michael J. Black. 2019. AMASS: Archive of Motion Capture as Surface Shapes. In *International Conference on Computer Vision*. 5442–5451.

Georgios Pavlakos, Vasileios Choutas, Nima Ghorbani, Timo Bolkart, Ahmed A. A. Osman, Dimitrios Tzionas, and Michael J. Black. 2019. Expressive Body Capture: 3D Hands, Face, and Body from a Single Image. In *Proceedings IEEE Conf. on Computer Vision and Pattern Recognition (CVPR)*. 10975–10985.

Ofir Press, Noah Smith, and Mike Lewis. 2022. Train Short, Test Long: Attention with Linear Biases Enables Input Length Extrapolation. In *International Conference on Learning Representations*. https://openreview.net/forum?id=R8sQPpGCv0

Davis Rempe, Tolga Birdal, Aaron Hertzmann, Jimei Yang, Srinath Sridhar, and Leonidas J. Guibas. 2021. HuMoR: 3D Human Motion Model for Robust Pose Estimation. In *International Conference on Computer Vision (ICCV)*.

Xiaolong Shen, Zongxin Yang, Xiaohan Wang, Jianxin Ma, Chang Zhou, and Yi Yang. 2023. Global-to-Local Modeling for Video-Based 3D Human Pose and Shape Estimation. In *Proceedings of the IEEE/CVF Conference on Computer Vision and Pattern Recognition (CVPR)*. 8887–8896.

Mingyi Shi, Kfir Aberman, Andreas Aristidou, Taku Komura, Dani Lischinski, Daniel Cohen-Or, and Baoquan Chen. 2020. Motionet: 3d human motion reconstruction from monocular video with skeleton consistency. *Acm transactions on graphics (tog)* 40, 1 (2020), 1–15.

Soyong Shin, Juyong Kim, Eni Halilaj, and Michael J Black. 2024. Wham: Reconstructing world-grounded humans with accurate 3d motion. In *Proceedings of the IEEE/CVF Conference on Computer Vision and Pattern Recognition*. 2070–2080.

Sebastian Starke, He Zhang, Taku Komura, and Jun Saito. 2019. Neural state machine for character-scene interactions. *ACM Transactions on Graphics* 38, 6 (2019), 178.

Jianlin Su, Murtadha Ahmed, Yu Lu, Shengfeng Pan, Wen Bo, and Yunfeng Liu. 2024. Roformer: Enhanced transformer with rotary position embedding. *Neurocomputing* 568 (2024), 127063.

Yu Sun, Qian Bao, Wu Liu, Tao Mei, and Michael J. Black. 2023. TRACE: 5D Temporal Regression of Avatars with Dynamic Cameras in 3D Environments. In *IEEE/CVF Conf. on Computer Vision and Pattern Recognition (CVPR)*.

Yu Sun, Yun Ye, Wu Liu, Wenpeng Gao, YiLi Fu, and Tao Mei. 2019. Human Mesh Recovery from Monocular Images via a Skeleton-disentangled Representation. In *IEEE International Conference on Computer Vision, ICCV*.

Zachary Teed and Jia Deng. 2021. DROID-SLAM: Deep Visual SLAM for Monocular, Stereo, and RGB-D Cameras. *Advances in neural information processing systems* (2021).

Zachary Teed, Lahav Lipson, and Jia Deng. 2024. Deep patch visual odometry. *Advances in Neural Information Processing Systems* 36 (2024).

Guy Tevet, Sigal Raab, Brian Gordon, Yoni Shafir, Daniel Cohen-or, and Amit Haim Bermano. 2023. Human Motion Diffusion Model. In *The Eleventh International Conference on Learning Representations*. https://openreview.net/forum?id=SJ1kSyO2jwu

Ashish Vaswani, Noam Shazeer, Niki Parmar, Jakob Uszkoreit, Llion Jones, Aidan N Gomez, Ł ukasz Kaiser, and Illia Polosukhin. 2017. Attention is All you Need. In *Advances in Neural Information Processing Systems*, I. Guyon, U. Von Luxburg, S. Bengio, H. Wallach, R. Fergus, S. Vishwanathan, and R. Garnett (Eds.), Vol. 30. Curran Associates, Inc. https://proceedings.neurips.cc/paper_files/paper/2017/file/3f5ee243547dee91fbd053c1c4a845aa-Paper.pdf

Timo von Marcard, Roberto Henschel, Michael Black, Bodo Rosenhahn, and Gerard Pons-Moll. 2018. Recovering Accurate 3D Human Pose in The Wild Using IMUs and a Moving Camera. In *European Conference on Computer Vision (ECCV)*.

Ziniu Wan, Zhengjia Li, Maoqing Tian, Jianbo Liu, Shuai Yi, and Hongsheng Li. 2021. Encoder-decoder with Multi-level Attention for 3D Human Shape and Pose Estimation. In *The IEEE International Conference on Computer Vision (ICCV)*.

Yufu Wang and Kostas Daniilidis. 2023. Refit: Recurrent fitting network for 3d human recovery. In *Proceedings of the IEEE/CVF International Conference on Computer Vision*. 14644–14654.

Yufu Wang, Ziyun Wang, Lingjie Liu, and Kostas Daniilidis. 2024. TRAM: Global Trajectory and Motion of 3D Humans from in-the-wild Videos. *arXiv preprint arXiv:2403.17346* (2024).

Wen-Li Wei, Jen-Chun Lin, Tyng-Luh Liu, and Hong-Yuan Mark Liao. 2022. Capturing Humans in Motion: Temporal-Attentive 3D Human Pose and Shape Estimation from Monocular Video. In *The IEEE Conference on Computer Vision and Pattern Recognition (CVPR)*.

Yufei Xu, Jing Zhang, Qiming Zhang, and Dacheng Tao. 2022. ViTPose: Simple Vision Transformer Baselines for Human Pose Estimation. In *Advances in Neural Information Processing Systems*.

Vickie Ye, Georgios Pavlakos, Jitendra Malik, and Angjoo Kanazawa. 2023. Decoupling Human and Camera Motion from Videos in the Wild. In *IEEE Conference on Computer*

Vision and Pattern Recognition (CVPR).

Xinyu Yi, Yuxiao Zhou, and Feng Xu. 2021. TransPose: Real-time 3D Human Translation and Pose Estimation with Six Inertial Sensors. *ACM Transactions on Graphics* 40, 4, Article 86 (08 2021).

Wanqi Yin, Zhongang Cai, Ruisi Wang, Fanzhou Wang, Chen Wei, Haiyi Mei, Weiye Xiao, Zhitao Yang, Qingping Sun, Atsushi Yamashita, et al. 2024. WHAC: World-grounded Humans and Cameras. *arXiv preprint arXiv:2403.12959* (2024).

Ri Yu, Hwangpil Park, and Jehee Lee. 2021. Human dynamics from monocular video with dynamic camera movements. *ACM Trans. Graph.* 40, 6, Article 208 (dec 2021),

14 pages. https://doi.org/10.1145/3478513.3480504

Ye Yuan, Umar Iqbal, Pavlo Molchanov, Kris Kitani, and Jan Kautz. 2022. GLAMR: Global Occlusion-Aware Human Mesh Recovery with Dynamic Cameras. In *Proceedings of the IEEE/CVF Conference on Computer Vision and Pattern Recognition (CVPR).*

Hongwen Zhang, Yating Tian, Yuxiang Zhang, Mengcheng Li, Liang An, Zhenan Sun, and Yebin Liu. 2023. PyMAF-X: Towards Well-aligned Full-body Model Regression from Monocular Images. *IEEE Transactions on Pattern Analysis and Machine Intelligence* (2023).
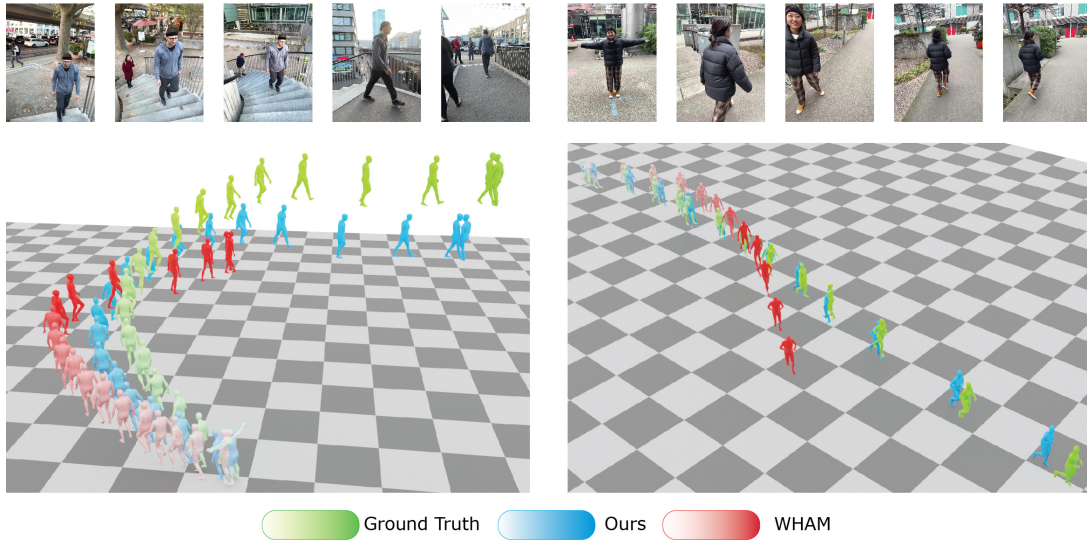
Fig. 7. **Qualitative results of global motion.** Our approach produces more accurate global motion than WHAM [Shin et al. 2024].
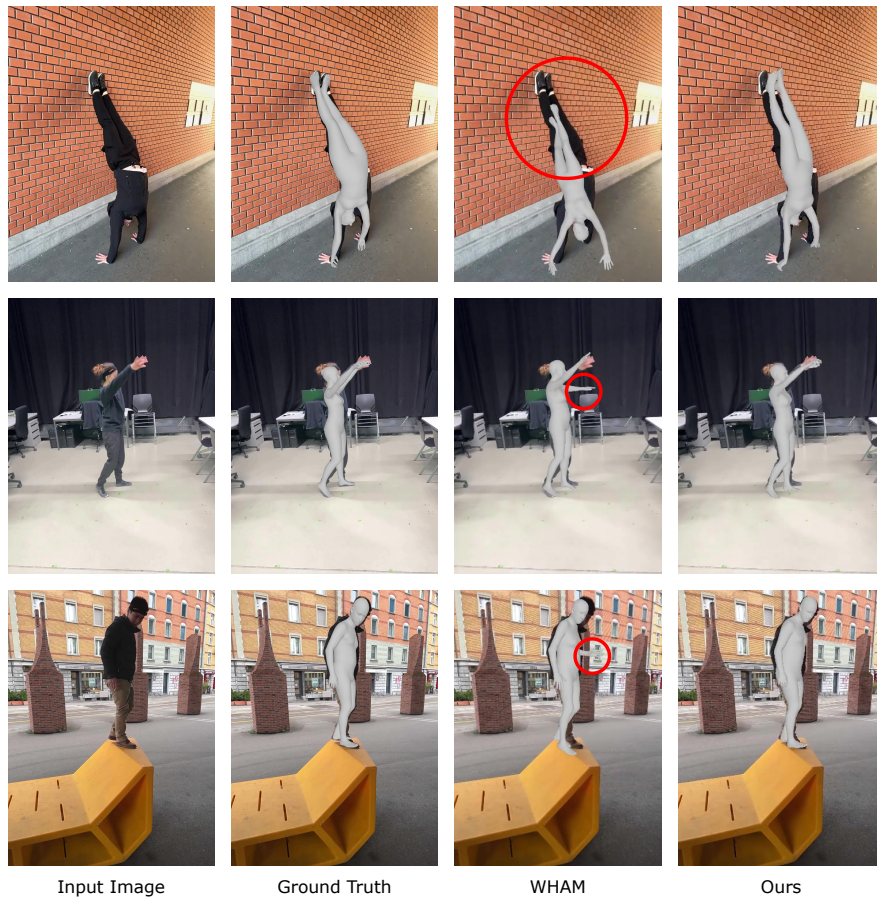

Fig. 8. **Qualitative results of motion in camera coordinates.** WHAM [Shin et al. 2024] could produce wrong results and fail to capture difficult motion (highlighted with red circles) while our approach could predict more plausible results.
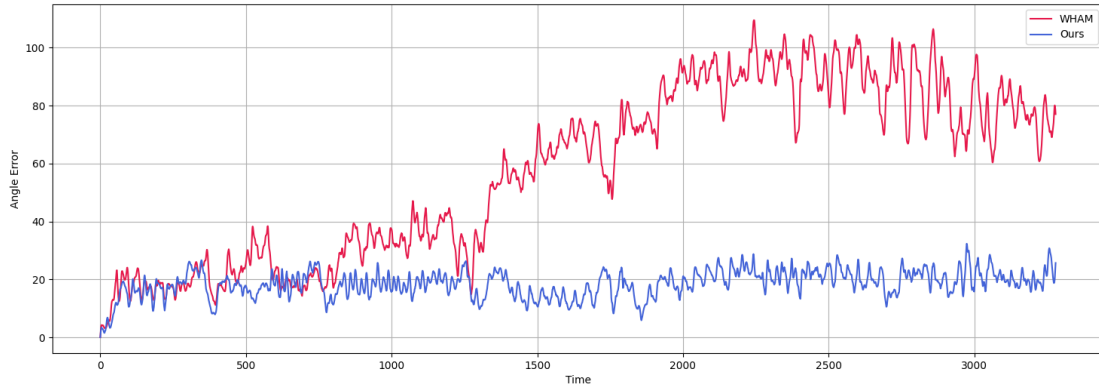
Fig. 9. **Global orientation error along time.** WHAM [Shin et al. 2024] tends to accumulate more global orientation error as the sequence length increases, while our approach maintains a much lower error rate.
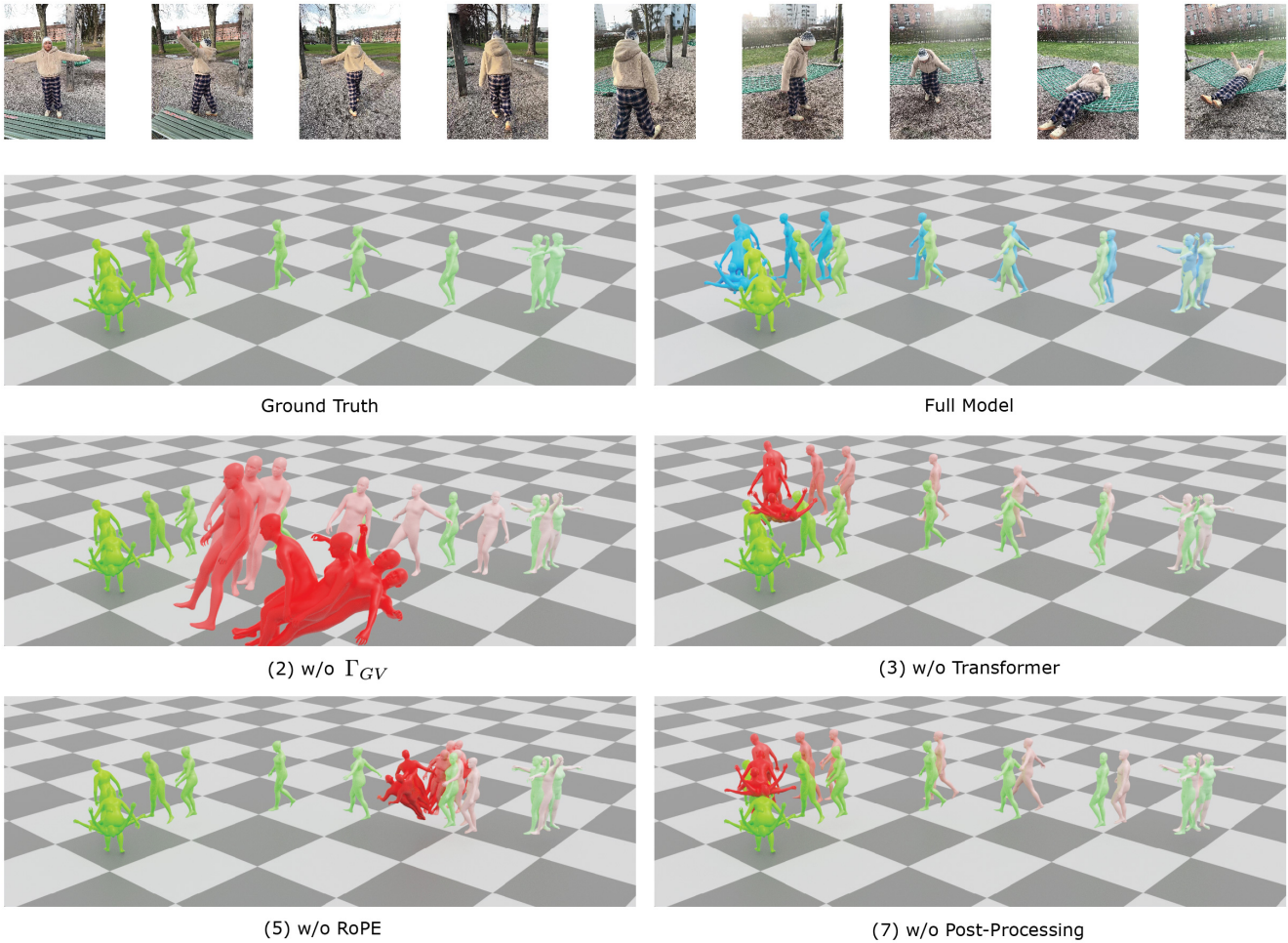

Fig. 10. **Qualitative results of ablations.** Each component of our method contributes to the final results.